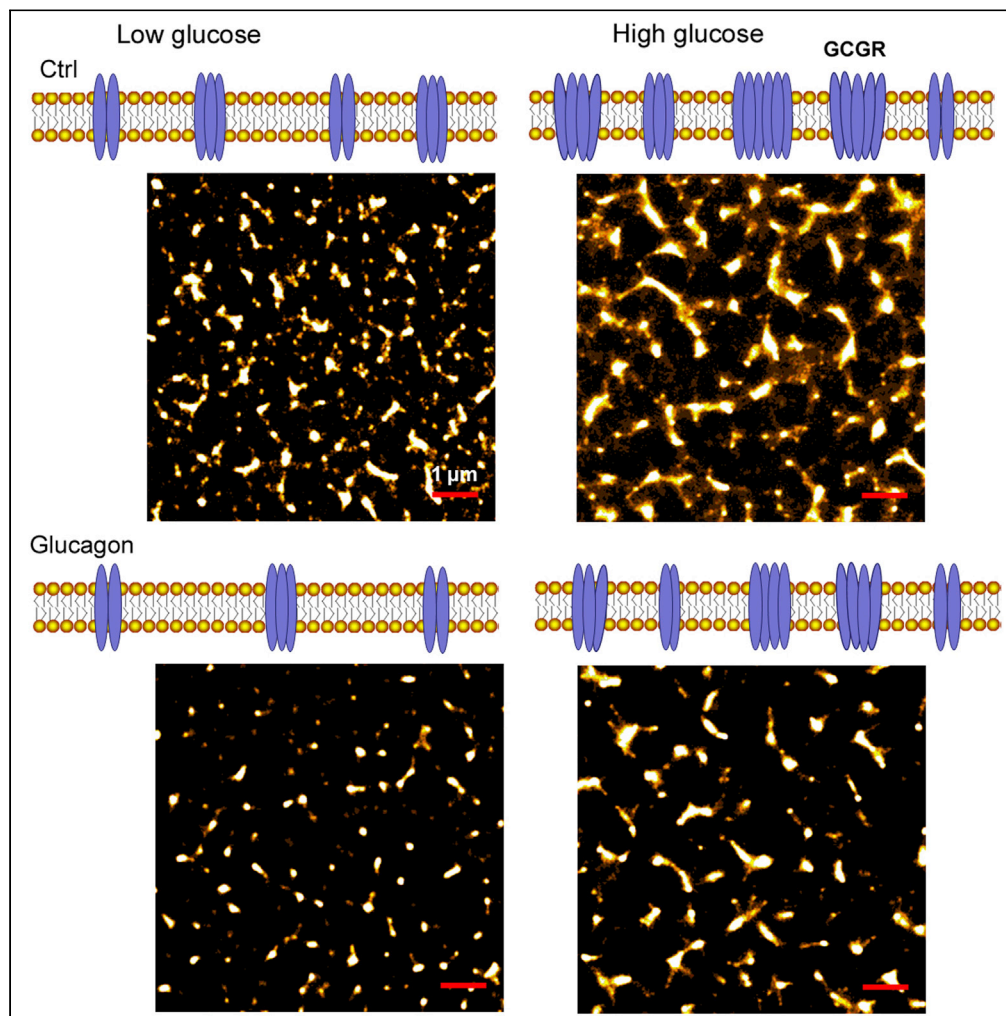


Article

High glucose-induced glucagon resistance and membrane distribution of GCGR revealed by super-resolution imaging



Jing Gao, Hongru Li, Haijiao Xu, ..., Yan Shi, Jingrui Zhang, Hongda Wang

gaojing@ciac.ac.cn (J.G.)
hdwang@ciac.ac.cn (H.W.)

Highlights

Nanoscale GCGR clusters were observed on HepG2 cell membranes by dSTORM imaging

High glucose promoted GCGR level and the formation of more and larger clusters

High glucose induced glucagon resistance of GCGR revealed by dSTORM imaging

High glucose induced stronger glucagon resistance in hepatoma cells

Gao et al., iScience 26, 105967
February 17, 2023 © 2023 The Author(s).
<https://doi.org/10.1016/j.isci.2023.105967>

Article

High glucose-induced glucagon resistance and membrane distribution of GCGR revealed by super-resolution imaging

Jing Gao,^{1,*} Hongru Li,^{1,2} Haijiao Xu,¹ Yong Liu,¹ Mingjun Cai,¹ Yan Shi,¹ Jingrui Zhang,¹ and Hongda Wang^{1,2,3,4,*}

SUMMARY

The glucagon receptor (GCGR) is a member of the class B G protein-coupled receptor family. Many research works have been carried out on GCGR structure, glucagon signaling pathway, and GCGR antagonists. However, the expression and fine distribution of GCGR proteins in response to glucagon under high glucose remain unclear. Using direct stochastic optical reconstruction microscopy (dSTORM) imaging, nanoscale GCGR clusters were observed on HepG2 cell membranes, and high glucose promoted GCGR expression and the formation of more and larger clusters. Moreover, glucagon stimulation under high glucose did not inhibit GCGR levels as significantly as that under low glucose and did not increase the downstream cyclic 3,5'-adenosine monophosphate-protein kinase A (cAMP-PKA) signal, and there were still large-size clusters on the membranes, indicating that high glucose induced glucagon resistance. In addition, high glucose induced stronger glucagon resistance in hepatoma cells compared with hepatic cells. Our work will pave a way to further our understanding of the pathogenesis of diabetes and develop more effective drugs targeting GCGR.

INTRODUCTION

The human glucagon receptor (GCGR) is a seven transmembrane-spanning class B G protein-coupled receptor (GPCR)^{1,2} and plays a key role in glucose homeostasis and the pathophysiology of type 2 diabetes.³ Once its ligand glucagon, a principal counter-regulatory hormone to insulin,^{4,5} binds to GCGR, it increases cyclic 3,5'-adenosine monophosphate (cAMP) levels via the activation of adenylyl cyclase through G α s and subsequently stimulates the protein kinase A (PKA) signaling pathway.^{6,7} The elevated PKA activity promotes glycogenolysis and gluconeogenesis and suppresses glycolysis and glycogen synthesis in the liver.⁸ Another mechanism is mediated via GCGR coupled to Gq, which regulates phospholipase C activities, inducing intracellular Ca²⁺ signaling and thus stimulating glycogenolysis and gluconeogenesis as well.^{9,10}

The driving force of continuous efforts to study GCGR is due to its important contribution in glucose release. As inhibition of GCGR activity can reduce excess glucose production, GCGR has been viewed as a crucial drug target for treatment of type 2 diabetes.¹¹ Since the early 1980s, GCGR antagonists have been reported in animal models,^{12,13} for clinical use, and recently also been confirmed in patients with type 2 diabetes.¹⁴ Considerable progress has been made in the identification of structural determinants of GCGR that are important for its ligand binding and the interaction with G proteins,^{15–17} in the development of potent small-molecule GCGR antagonists or antibodies,^{18,19} and in the unpicking of glucagon signaling pathways and the downstream effects in the liver.^{20,21} The expression of GCGR gene is regulated by many factors. Glucose, glucagon, cAMP, hepatic steatosis, exercise, age, and oxygen concentration all can affect the GCGR mRNA level in mouse liver.^{22–24} However, in terms of GCGR proteins, their fine distribution and spatial arrangement on the cell membranes remain unclear. Especially in response to glucagon or cAMP-related agents, the effect of chronic high glucose on the expression and distribution of GCGR proteins on liver cell membranes is not fully known. As glucagon hypersecretion is one of the most important causes of diabetes, solving these problems is a key to furthering our understanding of the pathogenesis of diabetes.

In order to investigate the spatial distribution and structural arrangement of membrane proteins at the single-molecule level, one of the super-resolution imaging techniques, direct stochastic optical

¹State Key Laboratory of Electroanalytical Chemistry, Changchun Institute of Applied Chemistry, Chinese Academy of Sciences, Research Center of Biomembranomics, Changchun, Jilin 130022, China

²University of Science and Technology of China, Hefei, Anhui 230027, China

³Laboratory for Marine Biology and Biotechnology, Qingdao National Laboratory for Marine Science and Technology, Wenhai Road, Aoshanwei, Jimo, Qingdao, Shandong 266237, China

⁴Lead contact

*Correspondence:

gaojing@ciac.ac.cn (J.G.),

hdwang@ciac.ac.cn (H.W.)

<https://doi.org/10.1016/j.isci.2023.105967>



reconstruction microscopy (dSTORM),²⁵ needs to be utilized. dSTORM relies on fluorophores that can be switched between a bright on and a dark off state. Only a few molecules are randomly excited to the bright on state, and their positions are recorded. By repeating this process, a reconstructed super-resolution image is finally obtained by accumulating the precise locations of each detected molecule. This approach allows direct observation of protein distribution with a resolution of decades of nanometer.^{26–28} Thus, dSTORM imaging is complementary to the traditional biochemical methods, and combining them is very beneficial for acquiring both overall and single-molecule information of GCGR's spatial distribution and expression regulation.

In this work, we investigated the effect of high glucose on GCGR membrane distribution and its downstream signaling by dSTORM imaging combined with western blotting. Furthermore, we observed the rearrangement of GCGR under glucagon stimulation and cAMP regulation and tested whether high glucose induced glucagon resistance. Ultimately, we elucidated different responses of GCGR to high glucose on hepatoma and hepatic cell membranes.

RESULTS AND DISCUSSION

Clustered distribution of GCGR on HepG2 cell membrane

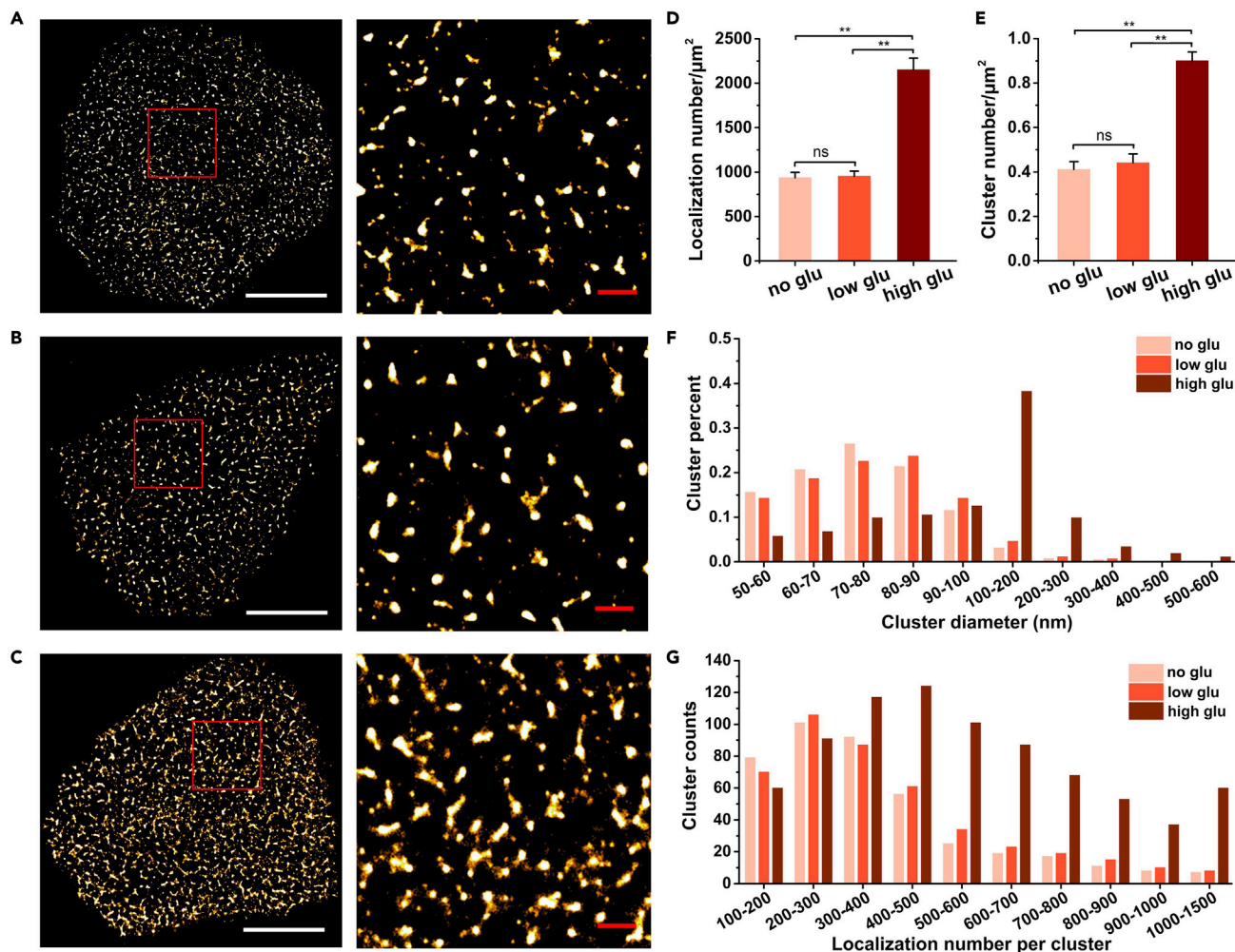
Glucagon receptor is mainly distributed in the human liver, so we chose to observe the GCGR distribution on HepG2 cell membranes by super-resolution fluorescence microscopy. The cells were cultured in no-glucose, low-glucose (5.5 mM), and high-glucose (25 mM) medium, and then the labeled samples were illuminated under the 647 nm laser. [Figures 1A–1C](#) show the distribution and morphology of GCGR on HepG2 cell membranes under different concentrations of glucose. In the case of no and low glucose, GCGR did not appear to aggregate significantly, while in the case of high glucose, GCGR appeared to be more and aggregate more intensively, which could be clearly observed in the enlarged images. From the statistical data, the localization number of GCGR under high glucose was more than twice that of no and low glucose ([Figure 1D](#)), which was proportional to the amount of proteins. The results suggested that high glucose promoted GCGR expression level on the membrane. The western blot assay showed that the total GCGR level was also greater under high glucose than that under low glucose ([Figures 6A and 6B](#)).

Furthermore, we analyzed the spatial distribution of GCGR by SR-Tesseler analysis method.²⁹ This method is based on Euclidean distances to divide regions and multiple thresholding of localization density to select qualified points (see [STAR Methods](#) for details). The results indicated that most of GCGR formed different sizes of clusters on the membranes under the three conditions. The cluster number under high glucose was twice as high as that under no and low glucose ([Figure 1E](#)). For the cluster diameter, it was mainly distributed in the range of 100–200 nm with high-glucose treatment, accounting for about 40% of the total clusters ([Figure 1F](#)). However, most of the clusters with no or low glucose had diameter less than 100 nm; 70–80 nm and 80–90 nm clusters occupied the highest proportion under no- and low-glucose condition, respectively ([Figure 1F](#)). In addition, when there is no or low glucose, the clusters with diameter of 200–300 nm were less than 5%, with 300–400 nm even less than 1%, and there were no clusters larger than 400 nm. More intriguingly, high glucose changed the molecular composition of GCGR clusters. For large clusters containing more than 300 localizations, the high-glucose group had twice or even several times more than the no- and low-glucose groups ([Figure 1G](#)). On the contrary, small clusters consisting of 100–300 localizations on cell membranes with no- or low-glucose treatment were more than those with high glucose ([Figure 1G](#)).

Collectively, these results indicate that GCGR forms different number and size of clusters on HepG2 cell membranes under different glucose concentration and high glucose regulates the redistribution of its clusters. High glucose not only increases the expression level of GCGR but also promotes it to form more and denser clusters.

High glucose leads to GCGR resistance to glucagon

High glucose can cause insulin resistance and increase the risk of liver cancer.^{30,31} However, the effect of high glucose on glucagon is rarely reported. As a glucagon receptor, it is unknown whether high glucose affects the response of GCGR to glucagon and its spatial distribution on cell membranes. Therefore, we treated HepG2 cells cultured in the different glucose concentration with glucagon. As shown in [Figure 2](#), the reconstructed dSTORM images and corresponding magnified images manifested that glucagon stimulation decreased GCGR clustering no matter under what glucose concentration it is. To further evaluate the spatial distribution and clustering of GCGR in detail, we firstly analyzed the changes of localization



number. In the case of no and low glucose, it fell by more than half with glucagon treatment; whereas it decreased by less than a quarter under high glucose after glucagon stimulation (Figure 3A). Similarly, western blot analysis showed that glucagon stimulation led the signal intensity of GCGR to be reduced by nearly half under low glucose but only about one-fifth under high glucose (Figures 6A and 6B). These results indicated that high glucose weakened the downregulation effect of glucagon stimulation on the expression level of GCGR.

Subsequently, we characterized GCGR clusters by SR-Tesseler analysis method as used above. The cluster number went down by almost 50% after adding glucagon under the condition of no and low glucose, while it only decreased by about 12% (from $0.89/\mu\text{m}^2$ to $0.78/\mu\text{m}^2$) under high glucose (Figure 3B). For cluster diameter, it became smaller after adding glucagon under both no and low glucose, and clusters with a diameter ranging from 60 nm to 70 nm occupied the greatest percentage (Figures 3C and 3D). The larger the diameter of the cluster was, the smaller the proportion was. And the largest cluster diameter is

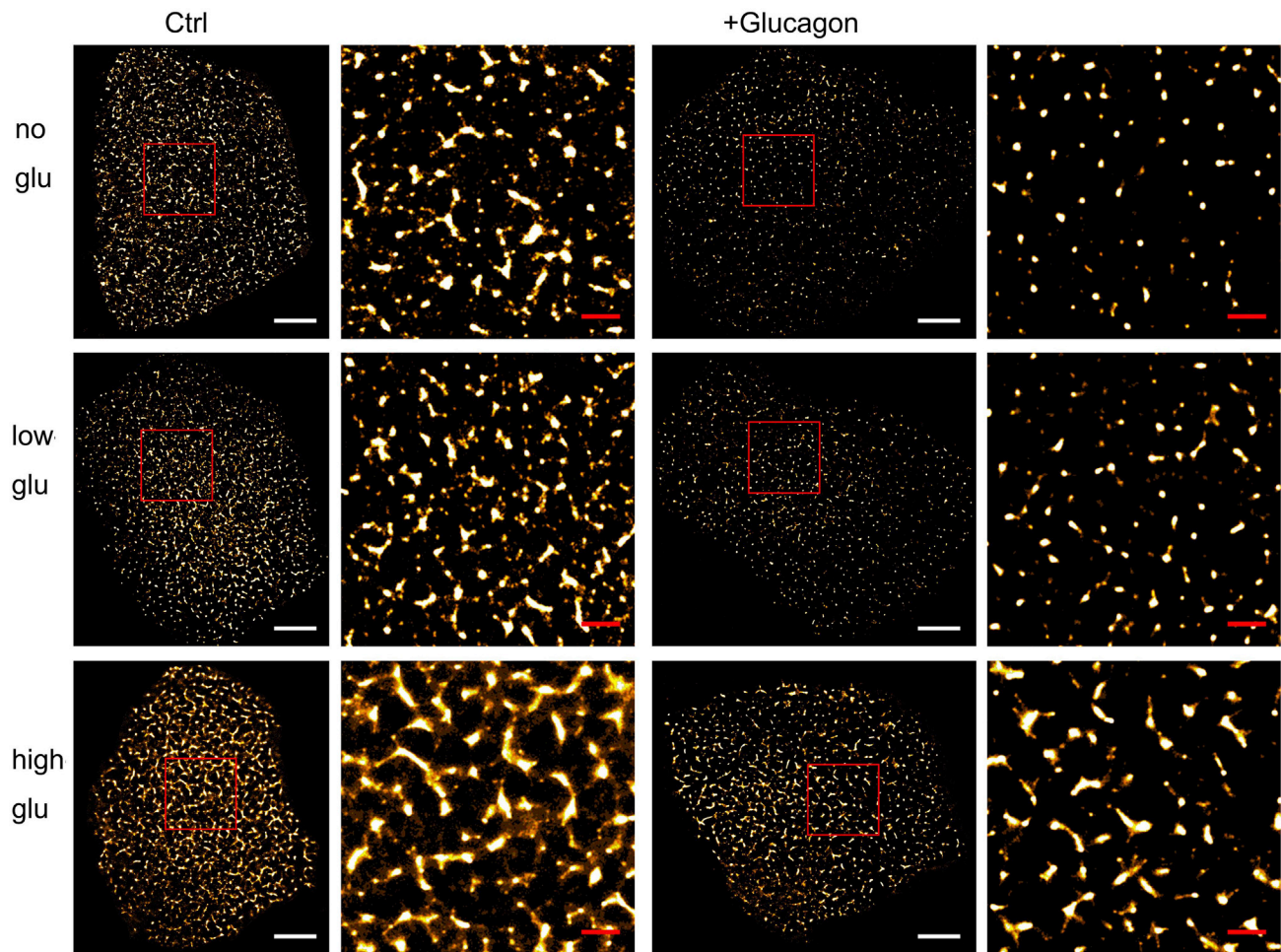


Figure 2. The distribution and clustering of membrane GCGRs following glucagon stimulation

The reconstructed dSTORM images of GCGR on HepG2 cell membranes with glucagon stimulation or left out and the corresponding zoomed-in regions (boxed in red). HepG2 cells were cultured without glucose (no glu), with 5.5 mM glucose (low glu), or with 25 mM glucose (high glu), respectively. Scale bars are 5 μm in the original images and 1 μm in the magnified images.

even less than 300 (low glucose) or 200 nm (no glucose). However, in the case of high glucose, clusters with 100–200 nm still accounted for the most, but the percentage decreased from 38% to 25%; and the proportion of clusters with small diameter (<100 nm) increased to a certain extent (Figure 3E). We also counted the molecular composition of clusters. Under no and low glucose, there was a significant reduction in the localization number per cluster with glucagon treatment, especially for clusters containing 200–500 localizations (Figures 3F and 3G). Under high glucose, clusters with less localization (<400) increased slightly, while clusters with more localizations (>500) decreased moderately (Figure 3H). These findings suggested that glucagon stimulation can reduce the formation and size of GCGR clusters under no- or low-glucose condition, but high glucose will hinder the negative regulation of glucagon on GCGR aggregation.

Moreover, we explored whether high glucose has an effect on the glucagon signaling pathway. As glucagon regulates blood glucose mainly through cAMP-PKA pathway in the liver, the expression of PKA and phosphorylated PKA was tested by western blot analysis (Figures 6A and 6C). Without glucagon, the level of p-PKA/PKA was higher under low glucose than that under high glucose. With glucagon treatment, there was an increase in the phosphorylation ratio under low glucose, whereas the ratio did not increase under high glucose. Although the expression of GCGR was higher under high glucose, its downstream signal level was weaker compared to that under low glucose.

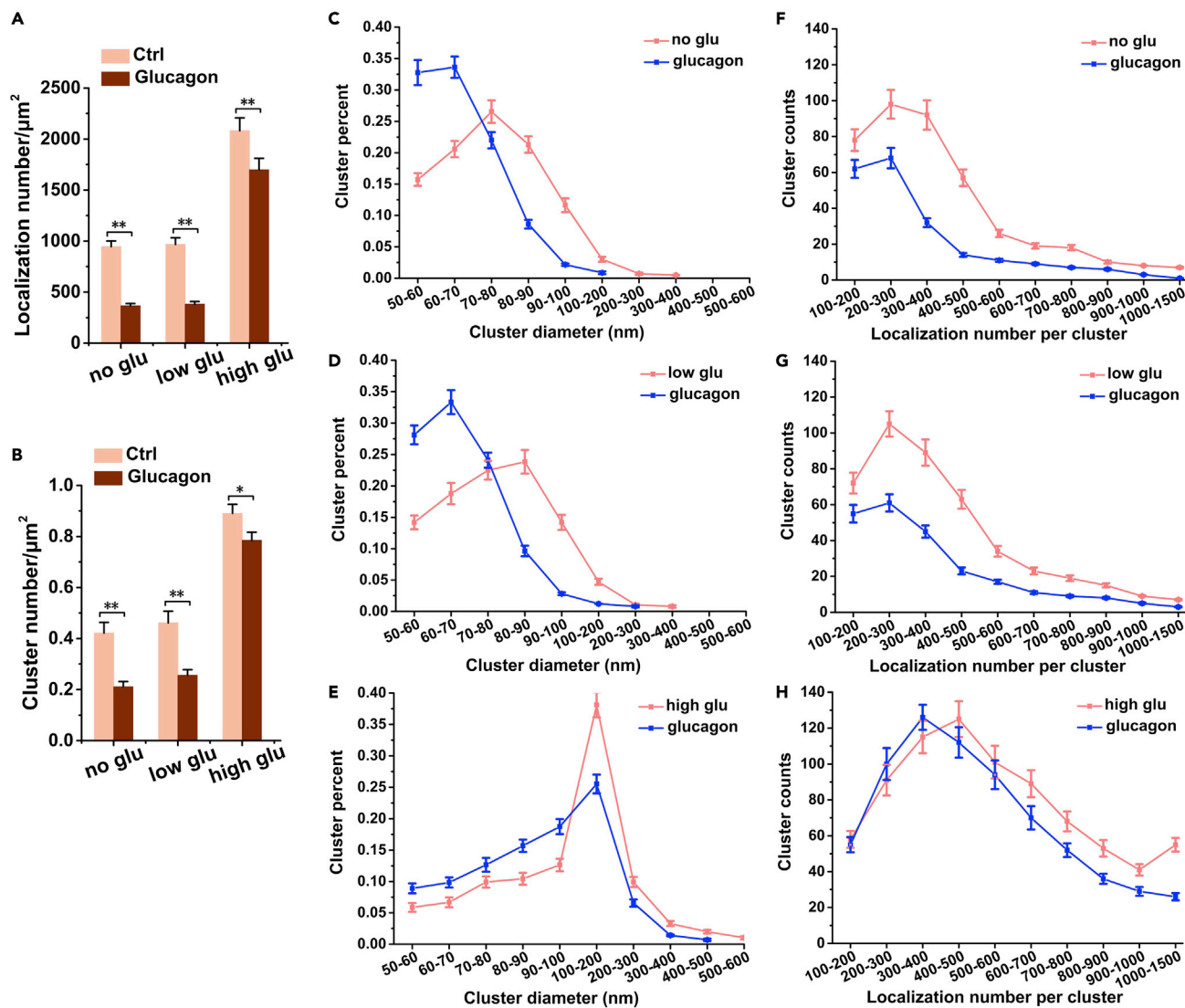


Figure 3. Cluster analysis of GCGR with glucagon stimulation

(A) The number of GCGR localizations per μm^2 with or without glucagon treatment under the condition of different glucose concentration.

(B) The number of clusters per μm^2 under the same condition as (A).

(C–E) The percentage of clusters with different cluster diameter without or with glucagon treatment under the condition of no glucose (C), low glucose (D), and high glucose (E).

(F–H) The distribution of localization number per cluster. Data shown are means \pm SD. All statistics were obtained from 20 cells in four independent experiments. *p < 0.05, **p < 0.01, two-tailed unpaired t test.

Taken together, high glucose made GCGR insensitive to the effect of glucagon, and the negative feedback inhibition of glucagon on GCGR was attenuated. Thus, with high glucose plus glucagon stimulation, the expression level of GCGR was higher and its aggregation on the liver cell membrane was more significant compared to that under low glucose. The downstream signal had no increasing trend after stimulation of glucagon, indicating that high-glucose environment can cause GCGR resistance and affect the glucose regulation function of glucagon. It is known that GCGR binds to glucagon and performs its function mainly by activating Gs protein. Some studies have shown that both the extracellular domain (ECD) and transmembrane domain (TMD) of class B GPCR participate in ligand binding.^{32,33} When GCGR is not activated, the interaction between its ECD and TMD interaction can inhibit the receptor activity; when combined with glucagon, the intrinsic activation characteristic of ECD can be released and GCGR can be changed from inhibition to activation. Therefore, we speculate that high glucose may enhance the interaction between

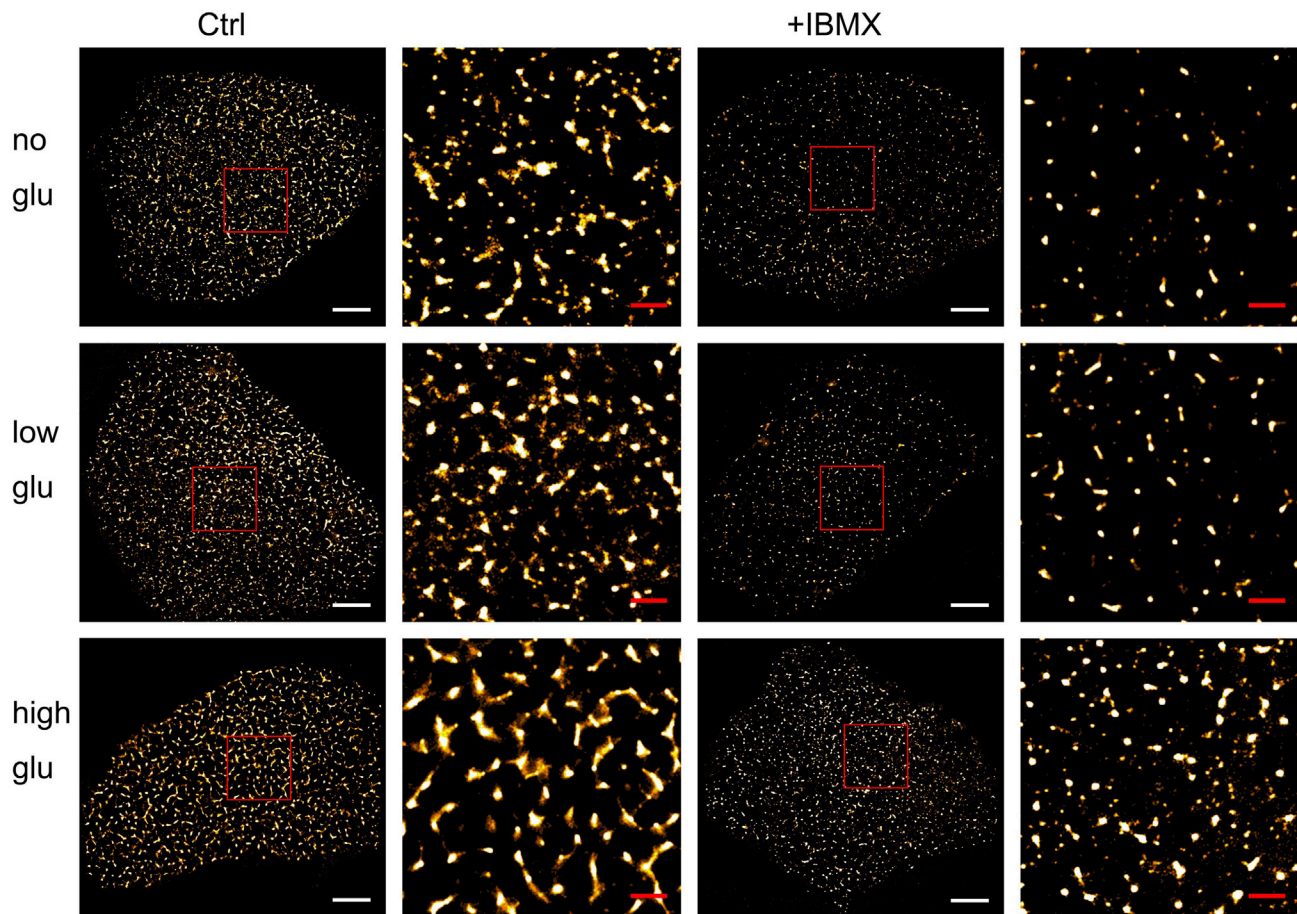


Figure 4. IBMX decreases levels of membrane GCGRs and inhibits their clustering

The reconstructed dSTORM images of GCGR on HepG2 cell membranes with IBMX treatment or left out and the corresponding zoomed-in regions (boxed in red). HepG2 cells were cultured with no, low, or high glucose, respectively. Scale bars are 5 μm in the original images and 1 μm in the magnified images.

ECD and TMD of GCGR or change the structure of ECD, thus reducing the binding of glucagon and its receptor. In order to maintain the activation of downstream signals, the number of GCGR and its clusters on the cell membrane increase with high glucose. Moreover, the negative feedback regulation of glucagon on GCGR level and clustering could become weaker than that under low glucose. However, it is necessary to analyze the structure of GCGR in high glucose to better reveal the interaction mode and activation mechanism of GCGR and ligand.

Increased cAMP levels inhibit GCGR clustering

Besides its own ligand glucagon, stimulus that leads to an increase in the production of cAMP can cause the suppression of GCGR transcription.^{22,34} For example, 3-isobutyl-1-methylxanthine (IBMX), a phosphodiesterase inhibitor, can raise cAMP production in hepatocytes and lower GCGR mRNA levels.³⁵ To further explore the effect of high glucose on the membrane distribution of GCGR proteins and downstream signaling, we treated HepG2 cells cultured in the different glucose concentration with IBMX. The reconstructed dSTORM images and corresponding magnified images showed that IBMX both lowered the GCGR protein levels and weakened its aggregation under the three glucose concentrations (Figure 4). Of note, at high glucose, the decrease of GCGR clustering seemed to be more obvious with IBMX treatment than with glucagon stimulation (Figures 2 and 4).

We firstly focused on the GCGR localization number after IBMX treatment. In the case of no and low glucose, it dropped to about one-third of that of control group (Figure 5A), which was similar to the situation with glucagon treatment (Figure 3A). However, it decreased by more than a half (from 2,112 to 887 per

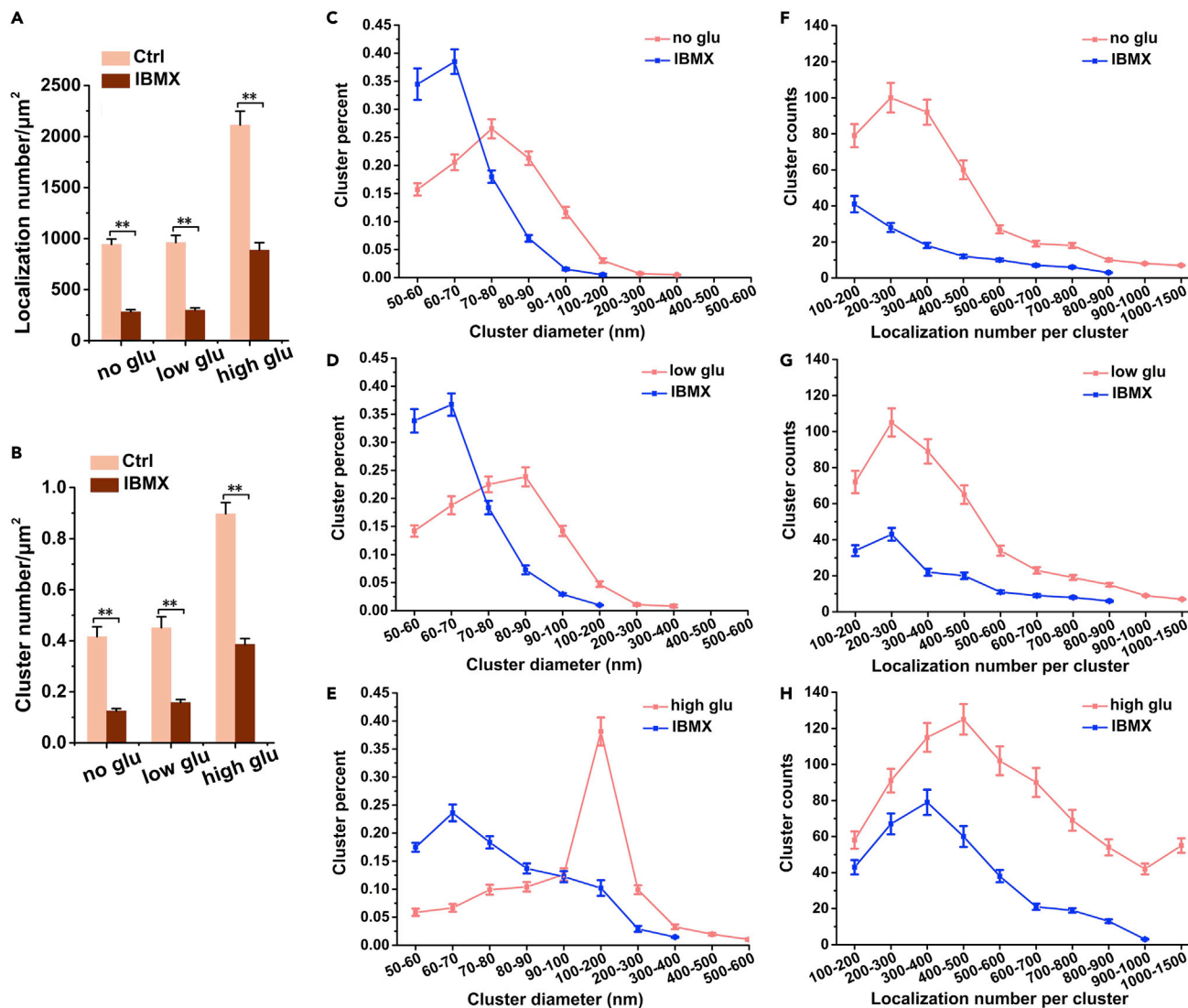


Figure 5. Cluster analysis of GCGR following IBMX treatment

(A) The number of GCGR localizations per μm^2 with or without IBMX treatment under the condition of different glucose concentration.

(B) The number of clusters per μm^2 .

(C–E) The percentage of clusters with different cluster diameter without or with IBMX treatment under the condition of no glucose (C), low glucose (D), and high glucose (E).

(F–H) The distribution of localization number per cluster. Data shown are means \pm SD. All statistics were obtained from 20 cells in four independent experiments. ** $p < 0.01$, two-tailed unpaired t test.

μm^2) under high glucose with IBMX, the decline rate of which was higher than that of glucagon stimulation (2,081 from to 1,700 per μm^2). The western blot analysis also showed the similar results (Figures 6A and 6B). The expression level of GCGR with either glucagon or IBMX treatment was reduced to 60% of that of the control group under low glucose (ctrl: glucagon: IBMX is 1: 0.64: 0.63); while under high glucose, glucagon lead to a decrease less than a quarter and IBMX resulted in a half decline (ctrl: glucagon: IBMX is 1.93: 1.55: 1.05). The results indicated that IBMX inhibited the expression of GCGR more significantly under high glucose than that under no or low glucose; and the inhibition was stronger than that with glucagon.

Next, we analyzed the clustering characteristic. For no and low glucose, the decrease of cluster number, diameter, and number of localizations in the cluster after IBMX treatment was roughly the same as that of glucagon stimulation (Figures 5B–5D, 5F, and 5G). For high glucose, the cluster number was reduced

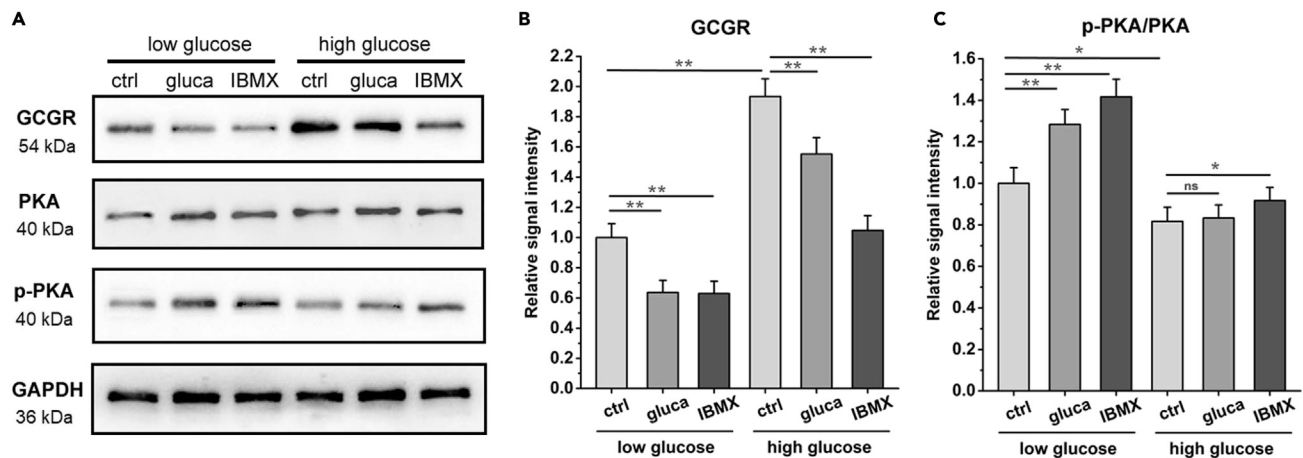


Figure 6. Effect of glucagon and IBMX on the expression of GCGR and cAMP-PKA signaling pathway

(A) Western blot analyses of GCGR, PKA, and phosphorylated PKA in HepG2 cells without or with glucagon and IBMX treatment under low- or high-glucose condition.

(B and C) The relative signal intensity of GCGR (B) and p-PKA/PKA (C) calculated after correction for the GAPDH loading control. Data shown are means \pm SD, from three independent experiments. * $p < 0.05$, ** $p < 0.01$, ns: no significance, two-tailed unpaired t test.

to less than a half with IBMX, and it was only about 12% with glucagon (Figures 3B and 5B). The cluster diameter also fell down dramatically. In the control group, clusters with the diameter of 100–200 nm accounted for the highest proportion; after the addition of IBMX, clusters with 60–70 nm diameter became the most (Figure 5E). However, when stimulated by glucagon, clusters at 100–200 nm still occupied the most, and only the percentage decreased (Figure 3E). Similarly, clusters with more localizations declined more pronouncedly with IBMX than with glucagon (Figures 5H and 3H). These results suggested that unlike glucagon, IBMX can inhibit the clustering of GCGR to some extent even in high glucose.

In addition, we also explored the effect of IBMX on glucagon signaling pathway. Under low glucose, the level of p-PKA/PKA increased remarkably with IBMX treatment, which was slightly higher than that with glucagon (Figures 6A and 6C). Under high glucose, the phosphorylation ratio had only increased a little with IBMX, but it was still statistically significant ($p < 0.05$), rather than no increase with glucagon. It is worth noting that, although the addition of IBMX under high glucose enhanced the downstream signal, the enhancement was far less than that under low glucose, and the expression of GCGR with high glucose plus IBMX was comparable to that of the control group under low glucose, indicating that high glucose made GCGR also have some resistance to cAMP regulation, but this resistance was weaker than that to glucagon.

It has been reported that increase of cAMP can lower GCGR mRNA levels. Our data showed that raise of cAMP suppressed GCGR protein level and clustering as well under normal conditions, whereas this repressing effect became stronger under high glucose and the downstream signal also increased slightly, demonstrating that high glucose can also inhibit the regulation of cAMP pathway on GCGR expression and membrane rearrangement. Moreover, we found that high glucose-induced GCGR was more insensitive to glucagon stimulation than increased cAMP. It might be because the glucagon stimulation did not significantly increase the cAMP production in high glucose, while the addition of IBMX directly affected cAMP to improve its level, which could be proved by the small increase of downstream phosphorylated PKA signal.

Effect of high glucose on GCGR distribution in hepatoma and hepatic cells

The metabolism of cancer cells is very different from that of normal cells. Cancer cells mainly supply energy through glycolysis. As a result, cancer cells use a lot of glucose in the body but generate little energy. So high glucose can increase a lot of energy and is found to be related to the incidence of liver cancer.^{30,31} Thus, we wanted to explore the difference of the effect of high glucose on the expression and distribution of GCGR in hepatoma and hepatic cells. In view of the fact that the expression and distribution of GCGR are basically the same under the conditions of no and low glucose (Figure 1), we only chose low and high glucose for comparison. Figure 7 showed the different distributions of GCGR on L-02 and HepG2 cell

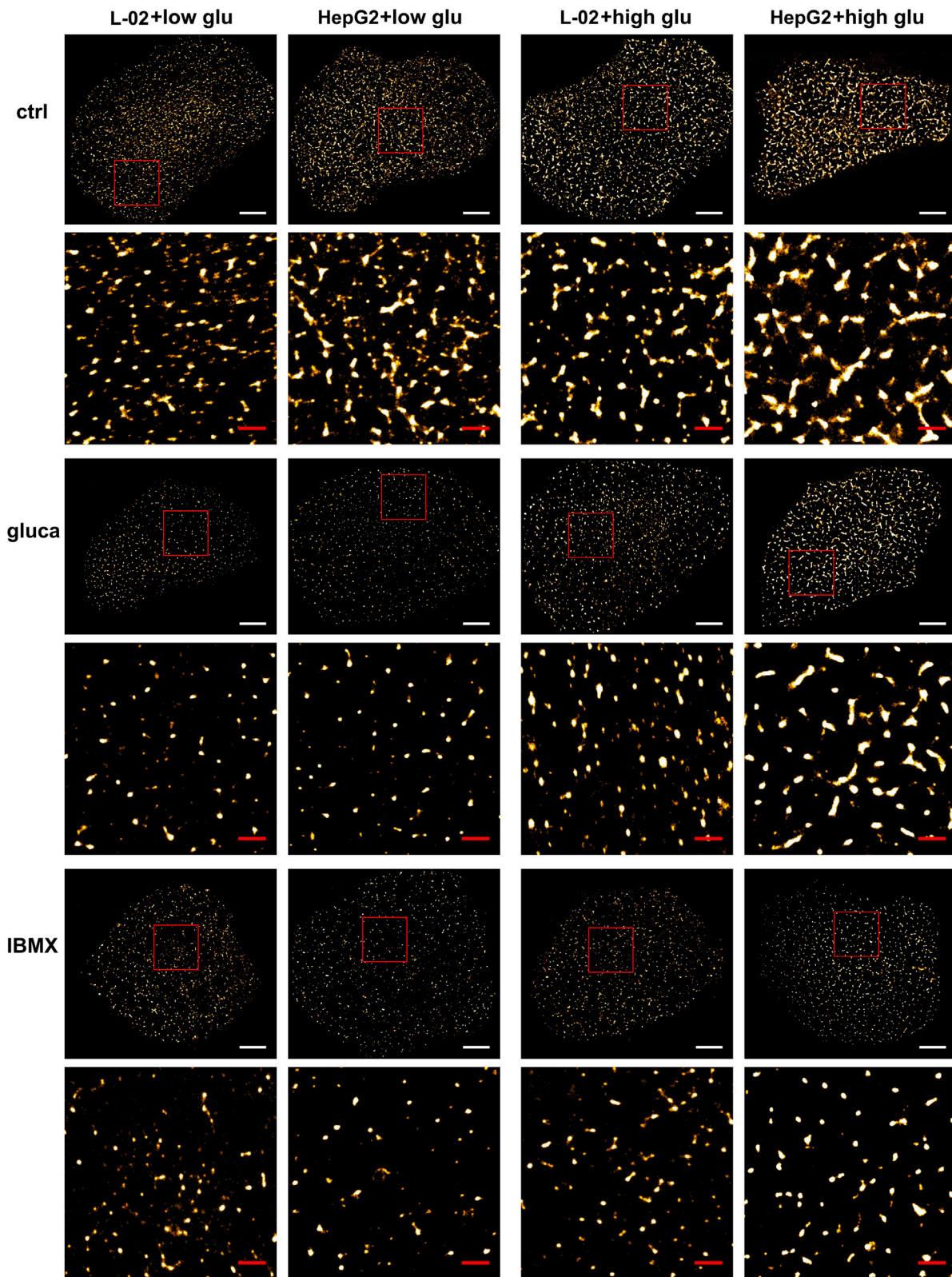


Figure 7. Super-resolution imaging of GCGRs on L-02 and HepG2 cell membranes induced by glucagon and IBMX under low- and-high glucose condition
Scale bars are 5 μm in the original images and 1 μm in the corresponding zoomed-in regions (boxed in red).

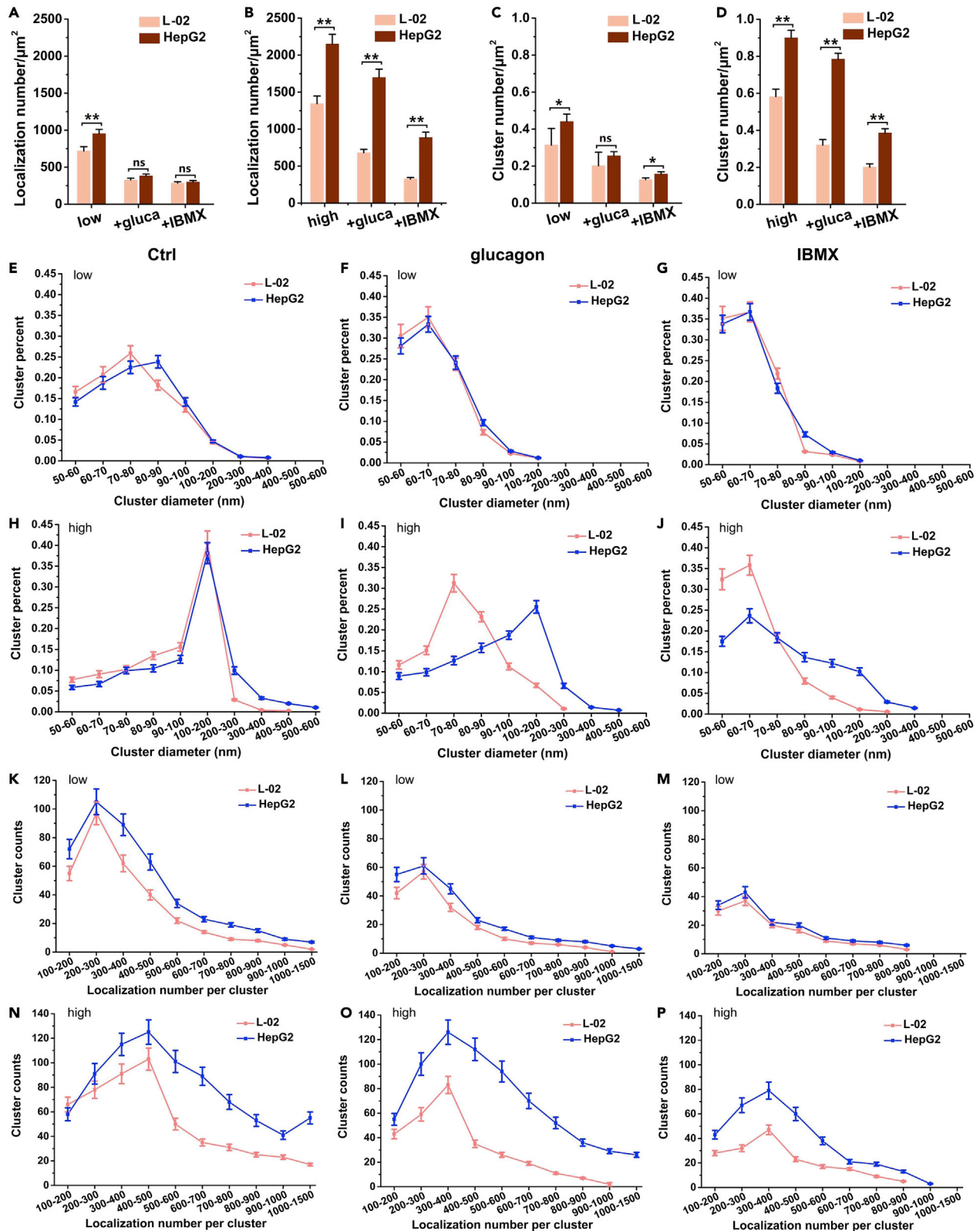


Figure 8. Cluster analysis of GCGR on L-02 and HepG2 cell membranes under different conditions

(A and B) The number of GCGR localizations per μm^2 on L-02 and HepG2 cell membranes under low- (A) or high-glucose (B) condition with glucagon or IBMX treatment.

(C and D) The number of clusters per μm^2 under low- (C) and high-glucose (D) condition.

(E–J) The percentage of clusters with different cluster diameter under the low (E–G) and high (H–J) glucose with nothing, glucagon or IBMX treatment.

(K–P) The distribution of localization number per cluster under the low (k-m) and high (n-p) glucose with different treatment. Data shown are means \pm SD. All statistics were obtained from 20 cells in four independent experiments. * $p < 0.05$, ** $p < 0.01$, ns means no significance, two-tailed unpaired t test.

membranes without or with glucagon and IBMX treatment under low and high glucose. To accurately assess the expression levels of GCGR, we quantitatively analyzed the number of localizations, which was proportional to the amount of proteins. Under low glucose, it was a little higher on HepG2 cells than that on L-02 cells without treatment and decreased to less than a half on both kinds of cells either with glucagon or with IBMX treatment (Figure 8A). Under high glucose, the localization number of HepG2 cells ($2,151 \pm 130$) was 1.5 times higher than that of L-02 cells ($1,344 \pm 105$) in the control group besides that both were higher than those under low glucose (Figure 8B). After glucagon or IBMX treatment, the decrease ratio of localization density in L-02 and HepG2 cells was 1:0.5:0.25 and 1:0.8:0.4 (ctrl: glucagon: IBMX), respectively. The results indicated that the change ratio of GCGR in the two kinds of cells was very similar under the three conditions in low glucose; however, high glucose increased the GCGR levels, especially in hepatoma cells, and led to stronger resistance of GCGR to glucagon in hepatoma cells than that in hepatic cells.

More intriguingly, we found that high glucose had different effects on the morphology and spatial distribution of GCGR on the two kinds of cells. We first analyzed the cluster number per μm^2 (Figures 8C and 8D). Its downward trend was similar to that of the localization density. The cluster number in HepG2 cells decreased less than that in L-02 cells when glucagon was added in high glucose. We next extracted the information of cluster diameter. Under low glucose, in the control HepG2 cells, the proportion of GCGR clusters with diameters of 80–90 nm was the highest, while in L-02 cells, 70–80 nm clusters were the most (Figure 8E). With glucagon or IBMX, the proportion of clusters with different sizes in the two kinds of cells was almost the same (Figures 8F and 8G). Under high glucose, in control groups, clusters with the diameter of 100–200 nm occupied the greatest percentage in both cells; however, HepG2 cells had more clusters with a diameter greater than 200 nm than L-02 cells (Figure 8H). Notably, the differences of cluster diameter between the two kinds of cells were more significant after adding glucagon or IBMX. For glucagon stimulation, the cluster diameter distribution of L-02 cells shifted to the left, showing a reduced cluster size (Figure 8I), while it did not change in HepG2 cells and only the proportion decreased. For IBMX addition, the cluster diameter decreased dramatically in both cells and clusters with 60–70 nm accounted for the largest percentage, but there were more larger clusters (diameter >80 nm) in HepG2 cells (Figure 8J). We also explored the molecular composition of clusters. The distribution of localization numbers in clusters in the two kinds of cells under low glucose was consistent in the three groups, and the difference was that HepG2 cells contained more clusters in each group (Figures 8K–8M). Similarly, glucagon and IBMX treatment significantly reduced large clusters with more localizations. On the contrary, control HepG2 cells under high glucose had more large clusters (especially for localizations >500) than L-02 cells (Figure 8N), and unlike L-02 cells, glucagon stimulation did not induce a remarkable decrease of localization number per cluster in HepG2 cells (Figure 8O). Even with IBMX treatment, the decline of HepG2 cells was also weaker than that of L-02 cells (Figure 8P).

Based on the above results, we found that the negative effect of high glucose on GCGR in hepatoma cells was deeper than that in hepatic cells, which mainly manifested in the stronger resistance to glucagon negative feedback, including no significant reduction in the expression level and clustering characteristic of GCGR. The results were in line with the high demand of cancer cell metabolism for glucose and suggested the importance and necessity of controlling high glucose, especially for patients with cancer.

Conclusions

In summary, using dSTORM imaging, we found that most of GCGRs were aggregated in clusters on HepG2 cell membranes under no or low glucose condition, whereas high glucose promoted the formation of more and larger clusters, accompanied by the increase of GCGR expression, which was also verified by western blot analysis. More importantly, glucagon stimulation in high glucose did not inhibit the expression of GCGR by negative feedback as significantly as that in low glucose and did not increase the downstream cAMP-PKA signal, either. Meanwhile, there were still large-size clusters with more molecules on the cell

membranes. These findings indicated that high glucose caused GCGR to resist glucagon and thus affected the normal glucose regulation of glucagon. When adding IBMX for raise of cAMP under high glucose, both GCGR protein levels and clustering reduced. However, the reduction was less than that of low glucose plus IBMX and more than that of high glucose plus glucagon. This might be because IBMX directly acted on cAMP, while glucagon did not, which could be confirmed by the strength of downstream phosphorylated PKA signal. This result revealed that high glucose also weakened the sensitivity of cAMP pathway in regulating GCGR expression and membrane distribution. Furthermore, we elucidated the differences of high-glucose regulation on GCGR in hepatoma and hepatic cells, that is, glucagon stimulation hardly reduced the level and aggregation of GCGR in hepatoma cells, which demonstrated that high glucose had a stronger negative effect on the regulation of blood glucose in hepatoma cells. Our work would allow a deeper understanding of the mechanism of high glucose-induced elevated GCGR expression, clustering, and glucagon resistance in the liver, and super-resolution fluorescence microscopy would shed new light on the study of the nanoscale spatial distribution and functions of membrane proteins.

Limitations of the study

In this study, we elucidated the clustered distribution of membrane GCGR at the nanometer scale and the effect of high glucose on GCGR expression, clustering, and glucagon resistance. Undoubtedly, continual efforts to unravel the mechanism of high glucose-induced glucagon resistance and GCGR clustering have promised to shed light on understanding the effects of glucose toxicity and the pathogenesis of diabetes. A crucial question regarding the relationship between protein clustering and downstream signal activation also needs to be investigated.

STAR★METHODS

Detailed methods are provided in the online version of this paper and include the following:

- [KEY RESOURCES TABLE](#)
- [RESOURCE AVAILABILITY](#)
 - Lead contact
 - Materials availability
 - Data and code availability
- [EXPERIMENTAL MODEL AND SUBJECT DETAILS](#)
 - Cell lines
- [METHOD DETAILS](#)
 - Sample pretreatment
 - Western blotting
 - Immunofluorescent staining
 - dSTORM imaging
 - dSTORM data analysis
- [QUANTIFICATION AND STATISTICAL ANALYSIS](#)

SUPPLEMENTAL INFORMATION

Supplemental information can be found online at <https://doi.org/10.1016/j.isci.2023.105967>.

ACKNOWLEDGMENTS

This work was financially supported by the National Natural Science Foundation of China (no. 22150003, 21727816, and 21721003 to H.W.) and the Scientific Instrument Developing Project of the Chinese Academy of Sciences (ZDKYYQ20220005 to H.W.).

AUTHOR CONTRIBUTIONS

J.G. designed and performed the research and wrote the paper. H.L. participated in cluster analysis. H.X., M.C., and Y.S. cultured cells and supplied the resources. J.Z. helped to perform western blotting analysis. H.W. supervised the research and revised the draft.

DECLARATION OF INTERESTS

The authors declare no competing interests.

INCLUSION AND DIVERSITY

We support inclusive, diverse, and equitable conduct of research.

Received: November 22, 2022

Revised: December 29, 2022

Accepted: January 10, 2023

Published: January 13, 2023

REFERENCES

- Jelinek, L.J., Lok, S., Rosenberg, G.B., Smith, R.A., Grant, F.J., Biggs, S., Bensch, P.A., Kuijper, J.L., Sheppard, P.O., Sprecher, C.A., et al. (1993). Expression cloning and signaling properties of the rat glucagon receptor. *Science* 259, 1614–1616. <https://doi.org/10.1126/science.8384375>.
- Mayo, K.E., Miller, L.J., Bataille, D., Dalle, S., Göke, B., Thorens, B., and Drucker, D.J. (2003). International union of pharmacology. XXXV. The glucagon receptor family. *Pharmacol. Rev.* 55, 167–194. <https://doi.org/10.1124/pr.55.1.6>.
- Burcelin, R., Katz, E.B., and Charron, M.J. (1996). Molecular and cellular aspects of the glucagon receptor: role in diabetes and metabolism. *Diabetes Metab.* 22, 373–396.
- Holst, J.J., Holland, W., Gromada, J., Lee, Y., Unger, R.H., Yan, H., Sloop, K.W., Kieffer, T.J., Diamond, N., and Herrera, P.L. (2017). Insulin and glucagon: partners for life. *Endocrinology* 158, 696–701. <https://doi.org/10.1210/en.2016-1748>.
- Müller, T.D., Finan, B., Clemmensen, C., DiMarchi, R.D., and Tschöp, M.H. (2017). The new biology and pharmacology of glucagon. *Physiol. Rev.* 97, 721–766. <https://doi.org/10.1152/physrev.00025.2016>.
- Habegger, K.M., Heppner, K.M., Geary, N., Bartness, T.J., DiMarchi, R., and Tschöp, M.H. (2010). The metabolic actions of glucagon revisited. *Nat. Rev. Endocrinol.* 6, 689–697. <https://doi.org/10.1038/nrendo.2010.187>.
- Rodgers, R.L. (2012). Glucagon and cyclic AMP: time to turn the page? *Curr. Diabetes Rev.* 8, 362–381.
- Quesada, I., Tudurí, E., Ripoll, C., and Nadal, A. (2008). Physiology of the pancreatic alpha-glucose secretion: role in glucose homeostasis and diabetes. *J. Endocrinol.* 199, 5–19. <https://doi.org/10.1677/joe-08-0290>.
- Aromataris, E.C., Roberts, M.L., Barritt, G.J., and Rychkov, G.Y. (2006). Glucagon activates Ca²⁺ and Cl⁻ channels in rat hepatocytes. *J. Physiol.* 573, 611–625. <https://doi.org/10.1113/jphysiol.2006.109819>.
- Jiang, Y., Cypess, A.M., Muse, E.D., Wu, C.R., Unson, C.G., Merrifield, R.B., and Sakmar, T.P. (2001). Glucagon receptor activates extracellular signal-regulated protein kinase 1/2 via cAMP-dependent protein kinase. *Proc. Natl. Acad. Sci. USA* 98, 10102–10107. <https://doi.org/10.1073/pnas.131200398>.
- Unger, R.H., and Cherrington, A.D. (2012). Glucagonocentric restructuring of diabetes: a pathophysiologic and therapeutic makeover. *J. Clin. Invest.* 122, 4–12. <https://doi.org/10.1172/jci60016>.
- Unson, C.G., Gurzenda, E.M., and Merrifield, R.B. (1989). Biological-activities of des-His1 [Glu9] glucagon amide, a glucagon antagonist. *Peptides* 10, 1171–1177. [https://doi.org/10.1016/0196-9781\(89\)90010-7](https://doi.org/10.1016/0196-9781(89)90010-7).
- Johnson, D.G., Goebel, C.U., Hruby, V.J., Bregman, M.D., and Trivedi, D. (1982). Hyperglycemia of diabetic rats decreased by a glucagon receptor antagonist. *Science* 215, 1115–1116. <https://doi.org/10.1126/science.6278587>.
- Kazda, C.M., Ding, Y., Kelly, R.P., Garhyan, P., Shi, C., Lim, C.N., Fu, H., Watson, D.E., Lewin, A.J., Landschulz, W.H., et al. (2016). Evaluation of efficacy and safety of the glucagon receptor antagonist LY2409021 in patients with type 2 diabetes: 12- and 24-week phase 2 studies. *Diabetes Care* 39, 1241–1249. <https://doi.org/10.1021/ac303064a>.
- Unson, C.G. (2002). Molecular determinants of glucagon receptor signaling. *Biopolymers* 66, 218–235. <https://doi.org/10.1002/bip.10259>.
- Christophe, J. (1995). Glucagon receptors - from genetic-structure and expression to effector coupling and biological responses. *Biochim. Biophys. Acta* 1241, 45–57. [https://doi.org/10.1016/0304-4157\(94\)00015-6](https://doi.org/10.1016/0304-4157(94)00015-6).
- Zhang, H., Qiao, A., Yang, D., Yang, L., Dai, A., De Graaf, C., Reedt-Runge, S., Dharmarajan, V., Zhang, H., Han, G.W., et al. (2017). Structure of the full-length glucagon class B G-protein-coupled receptor. *Nature* 546, 259–264. <https://doi.org/10.1038/nature22363>.
- Jiang, G., and Zhang, B.B. (2003). Glucagon and regulation of glucose metabolism. *Am. J. Physiol. Endocrinol. Metab.* 284, E671–E678. <https://doi.org/10.1152/ajpendo.00492.2002>.
- Kim, R.M., Chang, J., Lins, A.R., Brady, E., Candelore, M.R., Dallas-Yang, Q., Ding, V., Dragovic, J., Iliff, S., Jiang, G., et al. (2008). Discovery of potent, orally active benzimidazole glucagon receptor antagonists. *Bioorg. Med. Chem. Lett.* 18, 3701–3705. <https://doi.org/10.1016/j.bmcl.2008.05.072>.
- Galsgaard, K.D., Pedersen, J., Knop, F.K., Holst, J.J., and Wewer Albrechtsen, N.J. (2019). Glucagon receptor signaling and lipid metabolism. *Front. Physiol.* 10, 413. <https://doi.org/10.3389/fphys.2019.00413>.
- Janah, L., Kjeldsen, S., Galsgaard, K.D., Winther-Sørensen, M., Stojanovska, E., Pedersen, J., Knop, F.K., Holst, J.J., and Wewer Albrechtsen, N.J. (2019). Glucagon receptor signaling and glucagon resistance. *Int. J. Mol. Sci.* 20, 3314. <https://doi.org/10.3390/ijms20133314>.
- Abrahamsen, N., Lundgren, K., and Nishimura, E. (1995). Regulation of glucagon receptor mRNA in cultured primary rat hepatocytes by glucose and cAMP. *J. Biol. Chem.* 270, 15853–15857. <https://doi.org/10.1074/jbc.270.26.15853>.
- Burcelin, R., Mrejen, C., Decaux, J.F., De Mouzon, S.H., Girard, J., and Charron, M.J. (1998). In vivo and in vitro regulation of hepatic glucagon receptor mRNA concentration by glucose metabolism. *J. Biol. Chem.* 273, 8088–8093. <https://doi.org/10.1074/jbc.273.14.8088>.
- Melançon, A., Gagnon, V., Milot, M., Charest, É., Foucher, D., Péronnet, F., Unson O'Brien, C.G., Asselin, E., and Lavoie, C. (2013). Liver Glucagon Receptors (GLUR): effect of exercise and fasting on binding characteristics, GLUR-mRNA, and GLUR protein content in rats. *Horm. Metab. Res.* 45, 716–721. <https://doi.org/10.1055/s-0033-1349853>.
- van de Linde, S., Löscherberger, A., Klein, T., Heidebreder, M., Wolter, S., Heilemann, M., and Sauer, M. (2011). Direct stochastic optical reconstruction microscopy with standard fluorescent probes. *Nat. Protoc.* 6, 991–1009. <https://doi.org/10.1038/nprot.2011.336>.
- Schermelleh, L., Ferrand, A., Huser, T., Eggeling, C., Sauer, M., Biehlmaier, O., and Drummen, G.P.C. (2019). Super-resolution microscopy demystified. *Nat. Cell Biol.* 21, 72–84. <https://doi.org/10.1038/s41556-018-0251-8>.
- Li, H., Zhang, J., Shi, Y., Zhao, G., Xu, H., Cai, M., Gao, J., and Wang, H. (2022). Mechanism of INSR clustering with insulin activation and resistance revealed by super-resolution imaging. *Nanoscale* 14, 7747–7755. <https://doi.org/10.1039/d2nr01051h>.
- Yan, Q., Lu, Y., Zhou, L., Chen, J., Xu, H., Cai, M., Shi, Y., Jiang, J., Xiong, W., Gao, J., and Wang, H. (2018). Mechanistic insights into GLUT1 activation and clustering revealed by super-resolution imaging. *Proc. Natl. Acad. Sci. USA* 115, 7033–7038. <https://doi.org/10.1073/pnas.1803859115>.

29. Levet, F., Hosy, E., Kechkar, A., Butler, C., Beghin, A., Choquet, D., and Sibarita, J.-B. (2015). SR-Tesseler: a method to segment and quantify localization-based super-resolution microscopy data. *Nat. Methods* *12*, 1065–1071. <https://doi.org/10.1038/nmeth.3579>.
30. Garcia-Compean, D., Jaquez-Quintana, J.O., Gonzalez-Gonzalez, J.A., and Maldonado-Garza, H. (2009). Liver cirrhosis and diabetes: risk factors, pathophysiology, clinical implications and management. *World J. Gastroenterol.* *15*, 280–288. <https://doi.org/10.3748/wjg.15.280>.
31. Kim, K., Choi, S., and Park, S.M. (2018). Association of fasting serum glucose level and type 2 diabetes with hepatocellular carcinoma in men with chronic hepatitis B infection: a large cohort study. *Eur. J. Cancer* *102*, 103–113. <https://doi.org/10.1016/j.ejca.2018.07.008>.
32. Zhao, L.-H., Yin, Y., Yang, D., Liu, B., Hou, L., Wang, X., Pal, K., Jiang, Y., Feng, Y., Cai, X., et al. (2016). Differential requirement of the extracellular domain in activation of class B G protein-coupled receptors. *J. Biol. Chem.* *291*, 15119–15130. <https://doi.org/10.1074/jbc.M116.726620>.
33. Qiao, A., Han, S., Li, X., Li, Z., Zhao, P., Dai, A., Chang, R., Tai, L., Tan, Q., Chu, X., et al. (2020). Structural basis of G(s) and G(i) recognition by the human glucagon receptor. *Science* *367*, 1346–1352. <https://doi.org/10.1126/science.aaz5346>.
34. Mortensen, O.H., Dichmann, D.S., Abrahamsen, N., Grunnet, N., and Nishimura, E. (2007). Identification of a novel human glucagon receptor promoter: regulation by cAMP and PGC-1 alpha. *Gene* *393*, 127–136. <https://doi.org/10.1016/j.gene.2007.01.023>.
35. Nishimura, E., Abrahamsen, N., Hansen, L.H., Lundgren, K., and Madsen, O. (1996). Regulation of glucagon receptor expression. *Acta Physiol. Scand.* *157*, 329–332. <https://doi.org/10.1046/j.1365-201X.1996.35258000.x>.
36. Ovesný, M., Krížek, P., Borkovec, J., Svindrych, Z., and Hagen, G.M. (2014). ThunderSTORM: a comprehensive ImageJ plug-in for PALM and STORM data analysis and super-resolution imaging. *Bioinformatics* *30*, 2389–2390. <https://doi.org/10.1093/bioinformatics/btu202>.
37. Nieuwenhuizen, R.P.J., Lidke, K.A., Bates, M., Puig, D.L., Grünwald, D., Stallinga, S., and Rieger, B. (2013). Measuring image resolution in optical nanoscopy. *Nat. Methods* *10*, 557–562. <https://doi.org/10.1038/nmeth.2448>.
38. Culley, S., Albrecht, D., Jacobs, C., Pereira, P.M., Leterrier, C., Mercer, J., and Henriques, R. (2018). Quantitative mapping and minimization of super-resolution optical imaging artifacts. *Nat. Methods* *15*, 263–266. <https://doi.org/10.1038/nmeth.4605>.
39. Ma, X., Zhang, Y., Gromada, J., Sewing, S., Berggren, P.O., Buschard, K., Salehi, A., Vikman, J., Rorsman, P., and Eliasson, L. (2005). Glucagon stimulates exocytosis in mouse and rat pancreatic alpha-cells by binding to glucagon receptors. *Mol. Endocrinol.* *19*, 198–212. <https://doi.org/10.1210/me.2004-0059>.
40. Horwitz, E.M., and Gurd, R.S. (1988). Quantitative-analysis of internalization of glucagon by isolated hepatocytes. *Arch. Biochem. Biophys.* *267*, 758–769. [https://doi.org/10.1016/0003-9861\(88\)90085-9](https://doi.org/10.1016/0003-9861(88)90085-9).
41. Gao, J., He, L., Zhou, L., Jing, Y., Wang, F., Shi, Y., Cai, M., Sun, J., Xu, H., Jiang, J., et al. (2020). Mechanical force regulation of YAP by F-actin and GPCR revealed by super-resolution imaging. *Nanoscale* *12*, 2703–2714. <https://doi.org/10.1039/c9nr09452k>.
42. Jing, Y., Zhou, L., Chen, J., Xu, H., Sun, J., Cai, M., Jiang, J., Gao, J., and Wang, H. (2020). Quantitatively mapping the assembly pattern of EpCAM on cell membranes with peptide probes. *Anal. Chem.* *92*, 1865–1873. <https://doi.org/10.1021/acs.analchem.9b03901>.

STAR★METHODS

KEY RESOURCES TABLE

REAGENT or RESOURCE	SOURCE	IDENTIFIER
Antibodies		
Anti-GCGR	Abcam	Cat# Ab75240
Anti-PKA	Invitrogen	Cat# PA5-17626
Anti-phospho Thr197-PKA	Invitrogen	Cat# 711615
Alexa Fluor 647 goat anti-rabbit	Invitrogen	Cat# A-21245; RRID: AB_2535813
Anti-GAPDH	Proteintech	Cat# 60004-1-Ig
HRP-conjugated goat anti-mouse IgG	Proteintech	Cat# SA00001-1
HRP-conjugated goat anti-rabbit IgG	Proteintech	Cat# SA00001-2
Chemicals, peptides, and recombinant proteins		
DMEM	Gibco	Cat# 11965092
RPMI 1640	Gibco	Cat# 11875093
FBS	Gibco	Cat# 26010074
Trypsin-EDTA	Gibco	Cat# 15400054
Penicillin/streptomycin	Invitrogen	Cat# 15140122
Glucagon	Tocris Bioscience	Cat# 6927
IBMX	Sigma-Aldrich	Cat# I7018
Paraformaldehyde	Sigma-Aldrich	Cat# 158127-100G
BSA	Sigma-Aldrich	Cat# A1933-5G
glucose oxidase	Sigma-Aldrich	Cat# G2133-250KU
Catalase	Sigma-Aldrich	Cat# C1345-10G
β -mercaptoethanol	Sigma-Aldrich	Cat# M6250-100 ML
TetraSpeck microsphere (100 nm)	Invitrogen	Cat# T7279
Critical commercial assays		
Micro BCA™ Protein Assay Kit	Thermo Scientific	Cat# 23235
Experimental models: Cell lines		
HepG2 cell line	Cell Bank of the Chinese Academy of Sciences, Shanghai, China	CSTR:19,375.09.3101HUMTCHu72; RRID: CVCL_0027
HL-7702 (L-02) cell line	Nanjing Cbioer Biosciences Company	CBP60224; RRID: CVCL_6926
Software and algorithms		
ImageJ	https://imagej.nih.gov/ij/	N/A
ThunderSTORM	Martin et al. ³⁶	https://code.google.com/p/thunder-storm/
Fourier ring correlation	Nieuwenhuizen et al. ³⁷	N/A
NanoJ-SQUIRREL	Culley et al. ³⁸	https://bitbucket.org/rhenriqueslab/nanoj-squirrel
SR-Tesseler analysis	Levet et al. ²⁹	http://www.iins.u-bordeaux.fr/team-sibarita-SR-Tesseler

RESOURCE AVAILABILITY

Lead contact

Further information and requests for resources and reagents should be directed to and will be fulfilled by the lead contact, Dr. Hongda Wang (hdwang@ciac.ac.cn).

Materials availability

This study did not generate new unique reagents.

Data and code availability

- Data: The data that support the findings of this study are available from the corresponding author upon reasonable request.
- Code: This paper does not report original code
- Availability statement: Any additional information required to reanalyze the data reported in this paper is available from the [lead contact](#) upon request.

EXPERIMENTAL MODEL AND SUBJECT DETAILS

Cell lines

HepG2 cell line (Cell Bank of the Chinese Academy of Sciences, Shanghai, China) was cultured in high glucose Dulbecco's Modified Eagle Medium (DMEM; Gibco) supplemented with 10% fetal bovine serum (FBS; Gibco) and 100 µg/mL penicillin/streptomycin (P/S; Invitrogen). HL-7702 (L-02) cell line was purchased from Nanjing Cobioer Biosciences Company and cultured in RPMI 1640 medium supplemented with 10% FBS and 100 µg/mL P/S. Both cell lines were maintained under a humidified atmosphere of 5% CO₂ at 37°C.

METHOD DETAILS

Sample pretreatment

Firstly, cells were incubated in no glucose and serum-free medium for 2 h. For the glucose studies, the cells were cultured in no glucose, low glucose (5.5 mM) and high glucose (25 mM) medium for 48 h prior to experiments. For the glucagon studies, the cells cultured in no, low or high glucose medium were treated with 10 nM glucagon³⁹ (6927, Tocris Bioscience, UK) for 15 min at 4°C. The low temperature was kept to inhibit the endocytosis of glucagon.⁴⁰ For the IBMX (3-isobutyl-1-methylxanthine) studies, the cells cultured in the above described medium were treated with 1 mM IBMX (I7018, Sigma-Aldrich, CN) for 24 h.

Western blotting

The Western blot analysis was performed according to the standard protocol. The following primary antibodies were used: anti-GCGR (ab75240, Abcam; 1:1500 dilution), anti-PKA (PA5-17626, Invitrogen; 1:1000 dilution), anti-phosphoThr197-PKA (711,615, Invitrogen; 1: 250 dilution), and anti-GAPDH (Proteintech, 60004-1-Ig; 1: 2000 dilution). HRP-conjugated affininure goat anti-mouse IgG (Proteintech, SA00001-1; 1: 4000 dilution) and goat anti-rabbit IgG (Proteintech, SA00001-2; 1: 4000 dilution) were used as the secondary antibodies. All protein values were normalized to GAPDH levels.

Immunofluorescent staining

After the glucose, glucagon or IBMX treatment, cells were rinsed with PBS and fixed with 4% paraformaldehyde for 15 min at room temperature. Then cells were incubated with the blocking solution (3% BSA in PBS) for 30 min at room temperature. Staining was performed incubating samples with the primary GCGR antibodies (2 µg/mL in 3% BSA) overnight at 4°C, and washed with PBS for three times. At last, samples were incubated with Alexa Fluor 647 goat anti-rabbit antibodies (2 µg/mL in 3% BSA; Thermo Fisher Scientific, A-21245) for 30 min at room temperature. After three washes, 50 µL imaging buffer containing Tris (50 mM, pH 8.0), NaCl (10 mM), glucose (10% w/v), glucose oxidase (500 µg/mL; Sigma), catalase (40 µg/mL; Sigma) and β-mercaptoethanol (1% v/v; Sigma) was dropped on a large microscope slide (24 mm × 50 mm, Fisher), and the small slide (22 mm × 22 mm, Fisher) where cells were seeded was covered on the large one and sealed with nail polish.

dSTORM imaging

dSTORM imaging was performed on a Nikon Ti-E microscope with a 100 × 1.49 NA TIRF lens (Nikon, Japan). The sample was illuminated in total internal reflection fluorescence (TIRF) mode. The 640 nm laser was used to excite fluorophores of Alexa Fluor 647, and the 405 nm laser was used to increase the number of on-state fluorophores by carefully controlling its irradiation intensity (<0.1 kW/cm²). All images were captured by a cooled EMCCD (Andor Ixon Ultra 888). 5000 images were collected for each cell with an internal time of 25 ms between frames to reconstruct a super-resolution image. TetraSpeck microspheres of

100 nm (Invitrogen) were embedded in the sample to correct x–y drift, and a focus lock was used to correct z drift.

dSTORM data analysis

Raw dSTORM image sequences were analyzed by ThunderSTORM,³⁶ a free available plug-in in ImageJ. The camera parameters were set before running the analysis. Then the imaging stacks were processed by a series of feature-enhancing filters to map the accurate positions of molecules in every frame. Next, post-processing was run to eliminate unqualified molecules with poor localization, merge reappearing molecules and correct lateral drift. Finally, a reconstructed dSTORM image with nanoscale resolution was obtained.

To detect the imaging resolution of our home-built instrument, Fourier ring correlation (FRC)³⁷ was used to compare two independently super-resolution images of the same field of view. It was calculated by an ImageJ plug-in named NanoJ-SQUIRREL.³⁸ A sequence of images was firstly separated into odd and even frames and generated two new equal-sized blocks. FRC analysis was run on each block and provided an FRC map showing an estimate of resolution across the whole image (Figure S1). The lowest FRC value represented the minimum resolution.

To characterize the spatial distribution of GCGR on cell membranes, SR-Tesseler analysis method was used as previously reported.^{41,42} Firstly, a file including the coordinates, intensity and sigma of molecules was loaded in the program. The reconstructed image was shown and the whole cell was selected as an ROI to analyze (Figure S2A). Secondly, bisectors between two closest localizations were drawn, and the ROI was segmented into many polygons with different number of localizations (Figure S2B). The localization density of a polygon was defined as $\delta i1$, and the average localization density of the total ROI was $\delta 0$. If $\delta i1 > \delta 0$, localizations in this polygon were picked up to create an 'object' (Figure S2C). Similarly, the localization density of an object was set as $\delta i2$, and the average of all objects was $\delta 1$. Thirdly, objects satisfied the requirement of $\delta i2 > \delta 1$ were extracted as clusters (Figure S2D). Finally, the area, the number of localizations, coordinates and morphological parameters of each cluster were exported.

QUANTIFICATION AND STATISTICAL ANALYSIS

In each condition, we performed four independent experiments and chose five sets of cell data in each experiment. Thus, 20 cells in total were analyzed in each group. We calculated the mean value and SE for the 20 cells. The p values for testing the statistical significance between two groups were determined by unpaired t-test.